On numerical properties of the ensemble Kalman filter for data assimilation ☆

Jia Li, Dongbin Xiu *

Department of Mathematics, Purdue University, West Lafayette, IN 47907, USA

ARTICLE INFO

ABSTRACT

Ensemble Kalman filter (EnKF) has been widely used as a sequential data assimilation method, primarily due to its ease of implementation resulting from replacing the covariance evolution in the traditional Kalman filter (KF) by an approximate Monte Carlo ensemble sampling. In this paper rigorous analysis on the numerical errors of the EnKF is conducted in a general setting. Error bounds are provided and convergence of the EnKF to the exact Kalman filter is established. The analysis reveals that the ensemble errors induced by the Monte Carlo sampling can be dominant, compared to other errors such as the numerical integration error of the underlying model equations. Methods to reduce sampling errors are discussed. In particular, we present a deterministic sampling strategy based on cubature rules (qEnKF) which offers much improved accuracy. The analysis also suggests a less obvious fact — more frequent data assimilation may lead to larger numerical errors of the EnKF. Numerical examples are provided to verify the theoretical findings and to demonstrate the improved performance of the qEnKF.

© 2008 Elsevier B.V. All rights reserved.

1. Introduction

Interest in data assimilation methods has been growing rapidly in the atmospheric and oceanic communities and beyond. Data assimilation addresses the problem of producing useful analyses and forecasts given imperfect dynamical models and observations. The most widely adopted approach is the Kalman filter, which is the optimal data assimilation method for dynamics with additive, state-independent Gaussian model and observation errors. See, for example, [14,3]. An attractive feature of the Kalman filter is its calculation of forecast and analysis error covariances, in addition to the forecasts and analysis themselves. In this way the Kalman filter produces estimates of forecast and analysis uncertainty, consistent with the dynamics and prescribed model and observation error statistics. However, the calculations of the error covariance can be challenging in practice due to the high computational cost. Furthermore, for nonlinear dynamics the Kalman filter requires linearization or closure approximation for the error covariance equation, resulting in the extended Kalman filter (for example [11,13]), and can severely limit the effectiveness of the method.

The ensemble Kalman filter (EnKF), proposed by Evensen in [7], addresses the problem associated with linearization or closure by using ensemble representations for the forecast and analysis error covariances. In its native formulation, the EnKF uses a pure Monte Carlo sampling when generating the initial ensemble, the model

noise and the measurement perturbations. Each member of the ensemble is then forwarded by the full nonlinear dynamics and analyzed via the standard Kalman filter analysis scheme.

Since its introduction in [7], the EnKF has become popular in a wide variety of application areas and resulted in several variations in practical implementations. See, for example, extensive reviews in [8,10]. It is understood that the ensemble size determines the accuracy of the EnKF and as the ensemble size increases the EnKF should converge to the exact Kalman filter. In practice it is often time consuming to evolve the (nonlinear) model dynamics numerically, and one can only afford an ensemble with finite, often small, size. Therefore the major source of numerical errors is the statistical error from the Monte Carlo sampling. As a result, efforts have been devoted to designing alternative sampling strategies to reduce the errors of Monte Carlo sampling [20,9,19].

The purpose of this paper is to analyze the numerical error contributions to the EnKF. We demonstrate rigorously that the errors consist of ensemble sampling errors, as well as discretizational errors for solving the model equations. Subsequently, the convergence of the EnKF to the exact Kalman filter is established. We also propose an alternative deterministic sampling strategy based on numerical cubature rule, termed as qEnKF, which can significantly reduce the ensemble sampling error. The error analysis also indicates more frequent data assimilation may cause larger numerical errors of the EnKF, regardless the specific sampling strategy. This less-than-obvious result suggests that in practice the quality of the EnKF estimates may not be improved by simply using more frequent assimilation (whenever measurements are available).

The rest of the paper is arranged as follows. A brief introduction of the Kalman filter and the EnKF is in Section 2. A detailed

---

* Corresponding author. Tel.: +1 765 496 2846.
E-mail address: dxiu@math.purdue.edu (D. Xiu).

numerical accuracy analysis of the EnKF is conducted in Section 3. Discussions on reduction of sampling errors, particularly via the qEnKF approach, are in Section 4. Numerical examples are presented in Section 5 to support the theoretical analysis and to demonstrate the performance of the qEnKF.

2. Data assimilation and (ensemble) Kalman filter

Let $\Psi^f \in \mathbb{R}^m$, $m \geqslant 1$, be a vector of *forecast* state variables that are modelled by a system of (ordinary) differential equations

$$\frac{d\Psi^f}{dt} = f(t, \Psi^f), \quad t \in (0, T], \tag{1}$$

with $T > 0$ and initial condition

$$\Psi^f(0) = \Psi_0. \tag{2}$$

The model (1) and (2) is obviously not a perfect model for the true physics and the forecast may not represent the true state variables $\Psi^t \in \mathbb{R}^m$ sufficiently well. If a set of *measurements* $d \in \mathbb{R}^\ell, \ell \geqslant 1$, are available as

$$d = H\Psi^t + \epsilon, \tag{3}$$

where $H : \mathbb{R}^m \to \mathbb{R}^\ell$ is a measurement operator relating the *true state* variables Ψ^t and the observation vector $d \in \mathbb{R}^\ell$, and $\epsilon \in \mathbb{R}^\ell$ are measurement errors. Note the measurement operator can be nonlinear, although it is written in a linear fashion here by following the traditional exposition for the (ensemble) Kalman filter.

The objective of data assimilation is to construct an optimal estimate of the true state, the *analyzed state* vector denoted as $\Psi^a \in \mathbb{R}^m$, based on the forecast Ψ^f and the observation d. In the ensemble Kalman filter, the modelling error in (1) is assumed to be a random process with zero mean and the initial condition (2) is expressed as a random quantity to account for the modelling uncertainty in initial conditions. That is, (2) becomes

$$\Psi_0 \triangleq \Psi(z), \qquad z \in \mathbb{R}^n, \quad n \geqslant 1, \tag{4}$$

where z is a set of independent random variables parameterizing the random initial condition with probability density function $\rho(z) : \mathbb{R}^n \to \mathbb{R}^+$. Subsequently, the forecast state variables become stochastic variables and can be parameterized by the same set of random variables, i.e.,

$$\Psi^f \triangleq \Psi^f(t, z) : [0, T] \times \mathbb{R}^n \to \mathbb{R}^m.$$

Note it is possible to add a noise term in (1) as a model for the modelling error. Here we restrict ourselves to the deterministic model (1).

2.1. The Kalman filter

Let $P^f \in \mathbb{R}^{m \times m}$ and $P^a \in \mathbb{R}^{m \times m}$ be the error covariance matrices for the forecasted and the analyzed estimate, defined as

$$\begin{aligned} P^f &= \mathbb{E}\left[(\Psi^f - \Psi^t)(\Psi^f - \Psi^t)^T\right], \\ P^a &= \mathbb{E}\left[(\Psi^a - \Psi^t)(\Psi^a - \Psi^t)^T\right], \end{aligned} \tag{5}$$

respectively, where the superscripts T denote matrix transpose, and $\mathbb{E}$ is expectation operator, i.e.,

$$\mathbb{E}[g] = \int g(z)\rho(z)dz.$$

Also let

$$R = \mathbb{E}\left[(d - H\Psi^t)(d - H\Psi^t)^T\right] = \mathbb{E}\left[(d - d^t)(d - d^t)^T\right] = \mathbb{E}\left[\epsilon\epsilon^T\right] \tag{6}$$

be the measurement error covariance matrix, where $d^t = H\Psi^t$ is the true (and unknown) observations. We assume that, as usual,

$$\mathbb{E}\left[(d - d^t)(H\Psi^f - H\Psi^t)^T\right] = 0.$$

In the standard Kalman filter, the analyzed estimate Ψ^a is determined by a linear combination of the measurement vector d and the forecasted state vector Ψ^f. The linear combination is chosen to minimize the variance in the analyzed estimate, and is given by

$$\Psi^a = \Psi^f + K(d - H\Psi^f), \tag{7}$$

where $K \in \mathbb{R}^{m \times \ell}$ is the *Kalman gain matrix*

$$K = P^f H^T (H P^f H^T + R)^{-1}. \tag{8}$$

The analyzed error covariance matrix is updated by

$$P^a = (I - KH)P^f(I - KH)^T + KRK^T = (I - KH)P^f, \tag{9}$$

where I is the identity matrix, and the forecast covariance matrix P^f needs to be forwarded in time via an equation derived from the state governing Eq. (1). In linear case this can be easily realized; in nonlinear case, however, linearization of the model equation or some closure approximation is required which results in severe limitations on the effectiveness of the filter.

2.2. The ensemble Kalman filter

In the ensemble Kalman filter, an ensemble of the forecasted state are generated, i.e.,

$$(\Psi^f)_i \triangleq \Psi^f(t, (z)_i), \quad i = 1, \ldots, N, \tag{10}$$

where $\{(z)_i\}_{i=1}^N$ is the ensemble of size N for the random vector in the initial model state (4). Similarly a set of ensemble for the observation is introduced as

$$(d)_i = d + (\epsilon)_i, \quad i = 1, \ldots, N. \tag{11}$$

Furthermore, one defines ensemble covariance matrices around the ensemble mean, i.e.,

$$\begin{aligned} P_e^f &\triangleq \overline{(\Psi^f - \overline{\Psi^f})(\Psi^f - \overline{\Psi^f})^T} \simeq P^f, \\ P_e^a &\triangleq \overline{(\Psi^a - \overline{\Psi^a})(\Psi^a - \overline{\Psi^a})^T} \simeq P^a, \end{aligned} \tag{12}$$

as an approximation of the exact covariance matrices. Here the overbar denotes the ensemble averages that approximate the expectation operator, i.e.,

$$\overline{g} = \frac{1}{N} \sum_{i=1}^N g((z)_i) \simeq \mathbb{E}[g]. \tag{13}$$

Note for covariance evaluations the normalization factor is $N - 1$ instead of N. Similarly the observation error covariance matrix is approximated as

$$R_e = \overline{\epsilon\epsilon^T} \simeq R. \tag{14}$$

The analysis step for the EnKF consists of the following updates performed on each of the model state ensemble members:

$$(\Psi^a)_i = (\Psi^f)_i + K_e((d)_i - H(\Psi^f)_i), \quad i = 1, \ldots, N, \tag{15}$$

where

$$K_e = P_e^f H^T (H P_e^f H^T + R_e)^{-1} \tag{16}$$

is the *ensemble Kalman gain matrix*. One of the major advantages of the EnKF is that it evolves each ensemble member via the fully nonlinear system (1) and avoids forwarding the error covariance matrices of the forecasted estimates.

3. Accuracy analysis of the EnKF

In this section we analyze numerical errors to the EnKF and establish convergence of the EnKF to the Kalman filter. We first

analyze the local truncation error (LTE), which demonstrates that the numerical errors of the EnKF stem from the finite size ensemble approximation and numerical simulation of the forecast model equation (1). Convergence of the EnKF to the KF is established by examining the global error, which reveals a less obvious fact in that the numerical errors of the EnKF can increase if data assimilation is conducted more frequently.

3.1. Notations

In this section we set the notations for error analysis. Note that the exposition of the Kalman filter is rewritten slightly differently for the convenience of our analysis. We also assume that the exact solution of the Kalman filter exists throughout this paper (though it may be difficult to obtain).

Let t_n, $n = 1, 2, \ldots$, be the nth update time when observations d_n are available. Let $0 = t_0 \leqslant t_1 < t_2 < \cdots$, and without loss of generality, we assume $\{t_n\}$ are equally distributed with

$$\Delta T = t_{n+1} - t_n \quad \forall n \geqslant 0. \tag{17}$$

We further partition the time interval $[t_n, t_{n+1}]$ into m equal sized sub-interval,

$$t_{n,j} = t_n + j \cdot \Delta t, \quad j = 0, \ldots, m, \ n = 0, 1, \ldots,$$

where $t_{n,0} = t_n$, $t_{n,m} = t_{n+1}$, and $\Delta t > 0$ is the step size with which a stable and accurate numerical scheme is employed to solve the deterministic forecast model (1). The numerical scheme is forwarded in time on the stencil $t_{n,j}$, $0 \leqslant j \leqslant m, n \geqslant 0$. Without loss of generality, we assume the scheme is a one-step method in the following form,

$$\widetilde{\Psi}^f_{n,j+1} = \widetilde{\Psi}^f_{n,j} + \Delta t \cdot \Phi(t_{n,j}, \widetilde{\Psi}^f_{n,j}; \Delta t), \quad 0 \leqslant j < m, \quad n \geqslant 0, \tag{18}$$

where $\widetilde{\Psi}^f$ is the numerical solution of Ψ^f and $\Phi(\cdot)$ is an *increment function* satisfying the consistency condition

$$\lim_{\Delta t \to 0} \Phi(t_{n,j}, \Psi^f_{n,j}; \Delta t) = f(t_{n,j}, \Psi^f_{n,j}),$$

where $f(\cdot, \cdot)$ is the right-hand-side of the mode Eq. (1).

The numerical implementation of the EnKF, denoted as $\widehat{\widetilde{\Psi}}^a$, is obtained via the following recurrent procedure to evolve over one time step from t_n to t_{n+1}:

- At t_n, use an ensemble of the *analyzed solution* $(\widehat{\widetilde{\Psi}}^a_n)_i = (\widehat{\widetilde{\Psi}}^a(t_n))_i$, $i = 1, \ldots, N$ as initial conditions. When $n = 0$, $(\widehat{\widetilde{\Psi}}^a_0)_i$ is the ensemble of the initial condition (4) of (1),
- For each ensemble member $i = 1, \ldots, N$, solve the forecast model (1) via the numerical scheme (18) forward in time till t_{n+1}, i.e.,

$$(\widehat{\widetilde{\Psi}}^f_{n+1})_i = (\widehat{\widetilde{\Psi}}^a_n)_i + \Delta t \sum_{j=0}^{m-1} \Phi(t_{n,j}, (\widehat{\widetilde{\Psi}}^f_{n,j})_i; \Delta t) \quad (\widehat{\widetilde{\Psi}}^f_{n,0})_i = (\widehat{\widetilde{\Psi}}^a_n)_i. \tag{19}$$

- Apply the EnKF analysis scheme (15) to each ensemble member of the forecast to obtain the analyzed estimate, i.e., for $i = 1, \ldots, N$,

$$(\widehat{\widetilde{\Psi}}^a_{n+1})_i = (\widehat{\widetilde{\Psi}}^f_{n+1})_i + K_e((d_{n+1})_i - H(\widehat{\widetilde{\Psi}}^f_{n+1})_i). \tag{20}$$

The procedure is repeated till the desired time level T is reached. The notation $\widetilde{\Psi}$ is chosen in such a way that the $\sim$ denotes numerical errors are introduced by solving the forecast model (1) via (18), and the $\wedge$ denotes statistical errors are introduced by using the EnKF (15). Throughout this paper we will assume there is no error in the implementation of the measurement operator H.

In the following sections we will examine the errors of the EnKF. Here error is defined as the difference between analyzed model state obtained by the numerical EnKF $\widetilde{\Psi}^a$ and the exact solution of the traditional Kalman filter Ψ^a. The error will be measured by the following norm, for a random vector or matrix $v(z)$,

$$\|v\| \triangleq \sum_{i=1}^{N} w_i \|(v)_i\|_q, \tag{21}$$

where $(v)_i = v((z)_i)$, $i = 1, \ldots, N$, are an ensemble of $v(z)$, $\|\cdot\|_q$ is the standard q-norm for matrices and vectors, and w_i, $i = 1, \ldots, N$, are integration weights such that

$$\sum_{i=1}^{N} w_i \cdot (v)_i \simeq \int v(z) \rho(z) \mathrm{d}z, \tag{22}$$

and satisfy

$$w_i > 0 \quad \forall i, \qquad \sum_{i=1}^{N} w_i = 1. \tag{23}$$

In the standard EnKF, $w_i \equiv 1/N \ \forall i$. Obviously, when v is deterministic, $\|v\| = \|v\|_q$. We remark that other kinds of matrix norms other than the q-norm can be readily adopted here.

Hereafter unless stated explicitly to avoid confusion, we will use v to represent the entire ensemble of the random quantity $v(z)$, i.e., $v \triangleq \{(v)_i\}_{i=1}^N$. This is employed for the clarity of exposition.

3.2. Local truncation error

We first examine local truncation error (LTE) for the numerical EnKF procedure. The LTE is defined as the error introduced by forwarding an ensemble of the exact analyzed solution Ψ^a for one time step ΔT via the numerical EnKF scheme.

Let us consider the time interval $[t_n, t_{n+1}]$, $n \geqslant 0$. Let $\Psi^a_n = \{(\Psi^a(t_n))_i\}_{i=1}^N$ be an ensemble of the exact estimated state vector at t_n. The exact estimated state at t_{n+1} via the Kalman filter is

$$\Psi^a_{n+1} = \Psi^f_{n+1} + K(d_{n+1} - H\Psi^f_{n+1}), \tag{24}$$

where the model forecast Ψ^f_{n+1} is obtained by the exact solution of (1) at t_{n+1} with initial condition of Ψ^a_n at t_n.

In the EnKF, by using the exact ensemble state Ψ^a_n as initial condition at t_n, the approximate estimated state vector at t_{n+1}, denoted as $\widehat{\varphi}^a_{n+1}$, is

$$\widehat{\varphi}^a_{n+1} = \widetilde{\Psi}^f_{n+1} + K_e(d_{n+1} - H\widetilde{\Psi}^f_{n+1}), \tag{25}$$

where the numerical scheme (19) is used to obtain $\widetilde{\Psi}^f_{n+1}$, i.e.,

$$\widetilde{\Psi}^f_{n+1} = \Psi^a_n + \Delta t \sum_{j=0}^{m-1} \Phi(t_{n,j}, \widetilde{\Psi}^f_{n,j}; \Delta t), \qquad \widetilde{\Psi}^f_{n,0} = \Psi^a_n. \tag{26}$$

Lemma 1 (Local truncation error). *By following the conditions listed above and defining the local truncation error (LTE) at t_{n+1} as*

$$e_{n+1} \triangleq \|\widehat{\varphi}^a_{n+1} - \Psi^a_{n+1}\|, \tag{27}$$

the following error bound exists:

$$e_{n+1} \leqslant \|M\| \cdot \|\epsilon_{\Delta t}\| + \|\Delta K\| \cdot \|\epsilon^f\| + \|\Delta K\| \cdot \|H\| \cdot \|\epsilon_{\Delta t}\|, \tag{28}$$

where

$$\begin{aligned} M &= I - KH, \\ \epsilon_{\Delta t} &= \widetilde{\Psi}^f_{n+1} - \Psi^f_{n+1}, \\ \Delta K &= K_e - K, \\ \epsilon^f &= d_{n+1} - H\Psi^f_{n+1}. \end{aligned} \tag{29}$$

If one further assumes the convergence of the numerical scheme (26) as $\|\epsilon_{\Delta t}\| \sim O(\Delta t^p)$, $p \geqslant 1$, as $\Delta t \to 0$, the convergence of the ensemble Kalman gain matrix K_e to the exact Kalman gain matrix K as $\|\Delta K\| \sim O(N^{-\alpha})$, $\alpha > 0$, as $N \to \infty$, and ϵ^f satisfies $\sigma \sim O(\|\epsilon^f\|)$, and K and H are bounded for all $t \geqslant 0$, then

$$e_{n+1} \sim O(\Delta t^p, \sigma N^{-\alpha}), \quad \Delta t \to 0, \ N \to \infty. \tag{30}$$

Proof. The difference between $\widehat{\widetilde{\varphi}}^a_{n+1}$ and the exact analyzed state Ψ^a_{n+1} can be expressed as

$$
\begin{aligned}
\widehat{\widetilde{\varphi}}^a_{n+1} - \Psi^a_{n+1} &= (\widetilde{\Psi}^f_{n+1} - \Psi^f_{n+1}) + (K_e - K)d_{n+1} - (K_e H \widetilde{\Psi}^f_{n+1} - KH\Psi^f_{n+1}) \\
&= (\widetilde{\Psi}^f_{n+1} - \Psi^f_{n+1}) + (K_e - K)d_{n+1} \\
&\quad - (K_e H \widetilde{\Psi}^f_{n+1} - K_e H \Psi^f_{n+1} + K_e H \Psi^f_{n+1} - KH\Psi^f_{n+1}) \\
&= (\widetilde{\Psi}^f_{n+1} - \Psi^f_{n+1}) + (K_e - K)d_{n+1} \\
&\quad - K_e H(\widetilde{\Psi}^f_{n+1} - \Psi^f_{n+1}) - (K_e - K)H\Psi^f_{n+1} \\
&= (I - K_e H)(\widetilde{\Psi}^f_{n+1} - \Psi^f_{n+1}) + (K_e - K)(d_{n+1} - H\Psi^f_{n+1}) \\
&= (I - KH - \Delta KH)(\widetilde{\Psi}^f_{n+1} - \Psi^f_{n+1}) + \Delta K(d_{n+1} - H\Psi^f_{n+1}).
\end{aligned}
$$

After taking norm the error bound (28) follows.

When K and H are bounded for all t, so does M, and the estimate (30) is the leading order of errors in (28), in the limit of small time step $\Delta t \to 0$ and large ensemble size $N \to \infty$. This completes the proof. □

Remark 1. The above result indicates that the accuracy of the EnKF can be improved via refining the numerical algorithm for the forecast model (1), by using smaller time step Δt and/or higher-order method with larger p, and increasing the ensemble size (N) to decrease statistical errors.

Remark 2. The error term ϵ^f from (29) describes the discrepancy between the measurements d and its predicted values by the forecast Ψ^f (without numerical errors), and can be estimated as

$$\|\epsilon^f\| \leqslant \|d - H\Psi^t\| + \|H\Psi^t - H\Psi^f\| \leqslant \|\epsilon\| + \|H\| \cdot \|(\Psi^t - \Psi^f)\|, \tag{31}$$

where ϵ is the measurement error (see (3). Therefore the error ϵ^f includes the measurement error ϵ and the modelling error ($\Psi^t - \Psi^f$).

3.3. Global truncation error

The global truncation error (GTE) at $t = t_{n+1}$ is defined as the difference between the exact state estimate Ψ^a_{n+1} obtained by the Kalman filter and the state estimate $\widehat{\widetilde{\Psi}}^a_{n+1}$ obtained by solving the EnKF numerically, i.e.,

$$E_{n+1} = \|\widehat{\widetilde{\Psi}}^a_{n+1} - \Psi^a_{n+1}\|. \tag{32}$$

To analyze the global error, we first define a one-step *global increment function* for the EnKF operation. For any interval $[t_n, t_{n+1}]$, $n \geqslant 0$, by following the procedure of the EnKF in Section 3.1, the approximate estimated state $\widehat{\widetilde{\Psi}}^a_{n+1}$ can be expressed as

$$\widehat{\widetilde{\Psi}}^a_{n+1} = \widehat{\widetilde{\Psi}}^a_n + \Delta T \cdot U_e(t_n, \widehat{\widetilde{\Psi}}^a_n, d_{n+1}; \Delta t, \Delta T), \quad n = 0, 1, \ldots, \tag{33}$$

where $U_e(\cdots)$ is the one-step global increment function which can be written by using (19) and (20),

$$
\begin{aligned}
U_e(t_n, \widehat{\widetilde{\Psi}}^a_n, d_{n+1}; \Delta t, \Delta T) &= M_e \frac{\Delta t}{\Delta T} \sum_{j=0}^{m-1} \Phi(t_{n,j}, \widehat{\widetilde{\Psi}}^f_{n,j}; \Delta t) \\
&\quad + \frac{K_e}{\Delta T}(d_{n+1} - H\widehat{\widetilde{\Psi}}^a_n),
\end{aligned} \tag{34}
$$

where

$$M_e = I - K_e H, \quad \widehat{\widetilde{\Psi}}^f_{n,0} = \widehat{\widetilde{\Psi}}^a_n, \quad \Delta t = \Delta T/m. \tag{35}$$

Lemma 2 (Lipschitz continuity). *Assume the numerical scheme (18) is stable and its increment function Φ is Lipschitz continuous with respect to the second argument with a constant Γ that is independent*

of Δt and the nodes $t_{n,j}$, $n \geqslant 0$, $0 \leqslant j < m$. *Furthermore, if the matrices K_e, H are bounded for all $t \geqslant 0$, then the global increment function U_e from (34) is Lipschitz continuous with respect to the second argument, with a constant Λ independent of t_n, Δt, and measurements d, but dependent on ΔT, that is,*

$$\exists h > 0, \exists \Lambda > 0 : \forall \Delta t \in (0, h], n \geqslant 0,$$

$$\|U_e(t_n, \widehat{\widetilde{u}}^a_n, d_{n+1}; \Delta t, \Delta T) - U_e(t_n, \widehat{\widetilde{v}}^a_n, d_{n+1}; \Delta t, \Delta T)\| \leqslant \Lambda \|\widehat{\widetilde{u}}^a_n - \widehat{\widetilde{v}}^a_n\|. \tag{36}$$

Proof. By following the definition of U_e in (34) we obtain

$$
\begin{aligned}
&\|U_e(t_n, \widehat{\widetilde{u}}^a_n, d_{n+1}; \Delta t, m) - U_e(t_n, \widehat{\widetilde{v}}^a_n, d_{n+1}; \Delta t, m)\| \\
&= \|M_e \frac{\Delta t}{\Delta T} \sum_{j=0}^{m-1} \left[\Phi(t_{n,j}, \widehat{\widetilde{u}}^f_{n,j}; \Delta) - \Phi(t_{n,j}, \widehat{\widetilde{v}}^f_{n,j}; \Delta t) \right] \\
&\quad - \frac{1}{\Delta T} K_e H(\widehat{\widetilde{u}}^a_n - \widehat{\widetilde{v}}^a_n)\| \\
&\leqslant \frac{1}{m} \|M_e\| \left(\sum_{j=0}^{m-1} \Gamma \cdot \|\widehat{\widetilde{u}}^f_{n,j} - \widehat{\widetilde{v}}^f_{n,j}\| \right) + \frac{\|K_e H\|}{\Delta T} \|\widehat{\widetilde{u}}^a_n - \widehat{\widetilde{v}}^a_n\|,
\end{aligned}
$$

where the Lipschitz continuity assumption on the increment function Φ has been used in the last inequality, and $\widehat{\widetilde{u}}^f_{n,j}$ and $\widehat{\widetilde{v}}^f_{n,j}$ are solved by the scheme (18) with initial conditions $\widehat{\widetilde{u}}^a_n$ and $\widehat{\widetilde{v}}^a_n$, respectively. The stability of the scheme (18) implies that the scheme possesses continuous dependence on initial conditions, that is, $\exists h > 0, \exists C > 0$, such that $\forall \Delta t \in (0, h]$, $n \geqslant 0$ and $0 \leqslant j \leqslant m$,

$$\|\widehat{\widetilde{u}}^f_{n,j} - \widehat{\widetilde{v}}^f_{n,j}\| \leqslant C \|\widehat{\widetilde{u}}^a_n - \widehat{\widetilde{v}}^a_n\|.$$

By letting

$$\Lambda = C \cdot \Gamma \max_t \|M_e\| + \frac{1}{\Delta T} \max_t \|K_e H\|, \tag{37}$$

the Lipschitz property (36) follows. This completes the proof. □

Remark 3. The result of (37) indicates that the Lipschitz constant is *inversely proportional* to the size of ΔT. Subsequently, when the EnKF data assimilation is conducted more frequently (i.e., with smaller ΔT), the global increment function U_e for the EnKF has larger Lipschitz constant. This will have an impact on the global numerical error of the EnKF, as shown in the following result.

Theorem 1 (Global truncation error and convergence). *Let $\widehat{\widetilde{\Psi}}^a_n$ be the numerical result of the analyzed state at t_n, obtained by the ensemble Kalman filter with initial ensemble $\widehat{\widetilde{\Psi}}^a_0$ at $t = 0$. Let Ψ^a_n be the exact analyzed state at t_n, obtained by the exact implementation of the Kalman filter and the exact solution of (1) with initial condition (4). Then the global truncation error of the EnKF satisfies*

$$E_n \triangleq \|\widehat{\widetilde{\Psi}}^a_n - \Psi^a_n\| \leqslant \left(E_0 + \sum_{k=1}^n e_k \right) \exp(\Lambda \cdot t_n), \tag{38}$$

where $E_0 = \|\widehat{\widetilde{\Psi}}^a_0 - \Psi_0\|$ is the error in the initial ensemble, e_k are the local truncation errors (27) at t_k, and $\Lambda > 0$ is the Lipschitz constant with respect to the second argument for the global increment function U_e defined in (36). Therefore, if the convergence of the local truncation error (28) holds and $E_0 = \|\widehat{\widetilde{\Psi}}^a_0 - \Psi_0\| \to 0$ as $N \to \infty$, then the EnKF method is convergent for any $\Delta T > 0$.

Proof. By following (33), for any interval $[t_{n-1}, t_n]$, $n \geqslant 1$, the numerical solution of the EnKF satisfies

$$\widehat{\widetilde{\Psi}}^a_n = \widehat{\widetilde{\Psi}}^a_{n-1} + \Delta T \cdot U_e(t_{n-1}, \widehat{\widetilde{\Psi}}^a_{n-1}, d_n; \Delta t, \Delta T), \quad n \geqslant 1. \tag{39}$$

On the other hand, following the definition of the local truncation error, the exact solution of the Kalman filter satisfies

$$\Psi_n^a = \Psi_{n-1}^a + \Delta T \cdot U_e(t_{n-1}, \Psi_{n-1}^a, d_n; \Delta t, \Delta T) + \tau_n, \quad n \geqslant 1, \tag{40}$$

where, by definition, $\|\tau_n\| = e_n$ is the local truncation error at t_n, defined in (27).

By subtracting (39) from (40) and taking norm, we obtain, for $n \geqslant 1$,

$$E_n \leqslant E_{n-1} + e_n + \Delta T \cdot \|U_e(t_{n-1}, \widehat{\widetilde{\Psi}}_{n-1}^a, d_n; \Delta t, \Delta T)$$
$$- U_e(t_{n-1}, \Psi_{n-1}^a, d_n; \Delta t, \Delta T)\|.$$

By applying the formula recursively to smaller n, we obtain

$$E_n \leqslant E_0 + \sum_{k=1}^{n} e_k + \Delta T \cdot \sum_{k=0}^{n-1} \|U_e(t_k, \widehat{\widetilde{\Psi}}_k^a, d_{k+1}; \Delta t, \Delta T)$$
$$- U_e(t_k, \Psi_k^a, d_{k+1}; \Delta t, \Delta T)\|.$$

The Lipschitz condition (36) results in the following inequality

$$E_n \leqslant E_0 + \sum_{k=1}^{n} e_k + \Delta T \cdot \Lambda \sum_{k=0}^{n-1} E_k. \tag{41}$$

And the result of (38) is obtained by applying the discrete Gronwall theorem. See, for example, Chapter 11 of [17]. (Note $t_n = n\Delta T$.) This completes the proof. □

Remark 4. The convergence of the EnKF to KF by refining the numerical solver for the forecast model (1) and increasing ensemble size N is intuitive. A subtlety in the result (38) is the influence of the data assimilation time step ΔT on the numerical accuracy of the EnKF. From (37) and (38) it is clear that a smaller ΔT results in a larger Lipschitz constant Λ and therefore a larger approximation error, which also grows as time evolves. In practice it is often desirable to assimilate data more frequently as long as enough measurements are available, so that the analyzed states may converge to the true state more quickly. However, more frequent assimilation (with smaller ΔT) may result in larger numerical errors in the EnKF and is undesirable. Hence the choice of the size of assimilation step ΔT in EnKF should be a balanced issue after taking into account both its positive and negative impacts on the quality of the numerical estimation of the true state.

4. Reduction of sampling errors

The analysis from the previous sections indicates that the numerical errors in the implementation of the EnKF consist of two components: the error $\epsilon_{\Delta t}$ for solving the model equation (1) numerically, and the statistical error for replacing the Kalman gain matrix K by an ensemble matrix K_e (see (28)).

Due to the large amount of existing work, the numerical error $\epsilon_{\Delta t}$ for a given system (1) is mostly well understood and in many cases can be controlled to a sufficiently small level. Subsequently more research efforts have been devoted to reduction of sampling errors in the EnKF. It is clear from (16) that the sampling errors stem from two sources: the errors in sampling the measurement perturbations by using R_e to replace R, and the errors in sampling the model states.

4.1. Reduction of measurement sampling errors

In Kalman filter analysis scheme, it is essential to treat the observations as random variables with a distribution of mean equal to the first-guess observations and covariance equal to R (see [2,9]). In the original EnKF approach, an ensemble of observations are generated, with an ensemble covariance matrix R_e (14) which introduces an additional approximation. To eliminate the sampling error in R_e, it is possible to design implementations of the analysis scheme where the perturbation of measurements is avoided. Here we briefly review the method developed in [20], where the ensemble mean and the deviations from the mean are updated separately. The forecast and analysis states can be written as follows:

$$(\Psi^f)_i = \overline{\Psi^f} + (\Psi^f)_i', \tag{42}$$
$$(\Psi^a)_i = \overline{\Psi^a} + (\Psi^a)_i', \quad i = 1, \ldots, N, \tag{43}$$

where $\overline{\Psi^f}$ and $\overline{\Psi^a}$ denote the mean of forecasted and analyzed states, and $(\Psi^f)_i'$ and $(\Psi^a)_i'$ are the corresponding deviations from the mean. The analysis step, following the notation of [20], is

$$\overline{\Psi^a} = \overline{\Psi^f} + K(d - H\overline{\Psi^f}), \tag{44}$$
$$(\Psi^a)_i' = (\Psi^f)_i' - \widetilde{K}H(\Psi^f)_i', \quad i = 1, \ldots, N, \tag{45}$$

where K is the Kalman gain matrix in the standard Kalman filter, and

$$\widetilde{K} = P^f H^T \left(\left(\sqrt{HP^f H^T + R} \right)^{-1} \right)^T \left(\sqrt{HP^f H^T + R} + \sqrt{R} \right)^{-1}, \tag{46}$$

which is obtained by solving the equation

$$(I - \widetilde{K}H)P^f(I - H^T\widetilde{K}^T) = (I - \widetilde{K}H)P^f, \tag{47}$$

so that the resulting covariance of the analysis states matches the theoretical covariance P^a in (9). Such an approach is termed the ensemble square root filter (EnSRF). More detailed discussions can be found in [1,9,20] and the review in [19].

4.2. Reduction of ensemble sampling errors

Most, if not all, EnKF approaches are based on pure Monte Carlo sampling of the model states. Therefore the ensemble error decreases as the ensemble size N increases, e.g., the sample mean has error proportional to $O(1/\sqrt{N})$. Such a rate of convergence is relatively slow, and accurate statistics can be obtained only with relatively large size of ensemble. In practice when the computational cost of the model simulation (1) is high one can only afford a finite, in many instances small, size of ensemble, the ensemble sampling error will be dominant. Sampling strategies for improved performance have been discussed, although they are still based on Monte Carlo sampling [16,15,9].

Here we present a deterministic sampling strategy based on cubature rules (qEnKF), for reduction of the ensemble sampling errors. The idea is that the ensemble average is an approximation to the expectation operator, which is an integral in terms of the independent random variables $z \in \mathbb{R}^n, n \geqslant 1$. See (13). Therefore one can take advantage of the existing research in multi-dimensional integrations where cubature rules are designed to approximate integrals accurately. The general form of a cubature rule, for a general function $v(z)$, takes the form of (22), where $(v)_i = v((z)_i)$ are the values of the function evaluated at a deterministic set of points of $\{(z)_i, i = 1, \ldots, N\}$, and $\{w_i\}_{i=1}^N$ are the integration weights. In qEnKF, the random ensemble used in the standard EnKF is replaced by the deterministic ensemble determined by a proper cubature rule. And the ensemble average (13) is replaced by the weighted sum of (22).

There is a large amount of literature on cubature rules, see, for example, the reviews in [4–6,12,18]. Here we emphasize that because the underlying mathematical model (1) can be highly nonlinear and complex and one often can only afford a finite size (N) of the repetitively computations of (1) it is essential to require the integration weights $\{w_i\}_{i=1}^N$ to be positive, as shown in (23), a condition that not all cubature rules satisfy. It is also desirable to have equal weights, i.e., $w_i = 1/N \; \forall i$, another condition that are not satisfied by many cubature rules. Here we propose to use the following cubature rules in qEnKF that satisfy the above conditions. For (22) with Gaussian probability density function

$$\rho(z) = \frac{1}{(\sqrt{2\pi})^n} e^{-z^T z/2}, \qquad z \in \mathbb{R}^n,$$

a set of $N = n + 1$ points

$$(z)_k = (z_{k,1}, z_{k,2}, \ldots, z_{k,n}), \quad k = 0, 1, \ldots, n \tag{48}$$

are defined as

$$z_{k,2r-1} = \sqrt{2} \cos\frac{2rk\pi}{n+1}, \quad z_{k,2r} = \sqrt{2}\sin\frac{2rk\pi}{n+1}, \quad r = 1, 2, \ldots, [n/2],$$

where $[n/2]$ is the greatest integer less than $n/2$, and if n is odd $z_{k,n} = (-1)^k$. The above cubature rule is called a degree-2 formula. That is, (22) is *exact* if $v(z)$ is any polynomials of degree up to two in term of the n-dimensional variable z.

Similarly, a cubature rule of degree three exists, which integrates any polynomials in term of z of degree up to three exactly. Such a rule consists of $N = 2n$ equally weighted points of

$$(z)_k = (z_{k,1}, z_{k,2}, \ldots, z_{k,n}), \quad k = 1, 2, \ldots, 2n, \tag{49}$$

with

$$z_{k,2r-1} = \sqrt{2}\cos\frac{(2r-1)k\pi}{n}, \quad z_{k,2r} = \sqrt{2}\sin\frac{(2r-1)k\pi}{n},$$
$$r = 1, 2, \ldots, [n/2],$$

and if n is odd $z_{k,n} = (-1)^k$.

The degree two and three formulas can be found in [21], where formulas for other type of probability density function $\rho(z)$ are also provided.

We remark that it is proved mathematically that the number of points $N = n + 1$ and $N = 2n$ for degree two and three formulas, respectively, is *minimal* for equally weighted cubature rules. In practice the performance of the above two rules is often better than the Monte Carlo method with much larger sampling points, even for relatively large dimensionality n.

5. Numerical examples

In this section we present numerical tests to verify the theoretical analysis in Section 3 and examine the performance of the qEnKF proposed in Section 4.2.

5.1. The model problem

Here we employ the model problem used in [9,10]. It is a one-dimensional linear advection model

$$\Psi_t + c\Psi_x = 0, \quad x \in [0, L], \ t > 0, \tag{50}$$

where the length of the domain is $L = 1000$ with periodic boundary condition, and the advection speed is $c = 1$. The grid spacing is $\Delta x = 1$ and the time step is $\Delta t = 1$. The true state Ψ^t is sampled from a Gaussian distribution, $\mathcal{N}$, with zero mean, unit variance, and a spatial de-correlation length of 20, which results in 50 equal-distance points of i.i.d. Gaussian random variables and a random space of 50 dimension, i.e., $z \in \mathbb{R}^n$ with $n = 50$. The first-guess solution is generated by drawing another sample from $\mathcal{N}$ and adding this to the true state. The initial ensemble is then generated by adding samples drawn from $\mathcal{N}$ to the first-guess solution. Thus, the initial state is assumed to have an error variance equal to one. Four measurements of the true solution, distributed evenly in the spatial domain, are assimilated every 5th time step, i.e., $\Delta T = 5$, with observation errors of zero mean and standard deviation of 0.1 unless stated otherwise. The observation errors are uncorrelated.

By using this simple model, the spatial and temporal discretization errors associated the numerical solver can be kept to minimum. This allows us to focus on the errors induced by various sampling strategies in the EnKF and its variations.

5.2. Results of the EnKF and EnSRF

We first examine the qualitative behavior of the EnKF. The results of the model problem is shown in Fig. 1. As expected, the
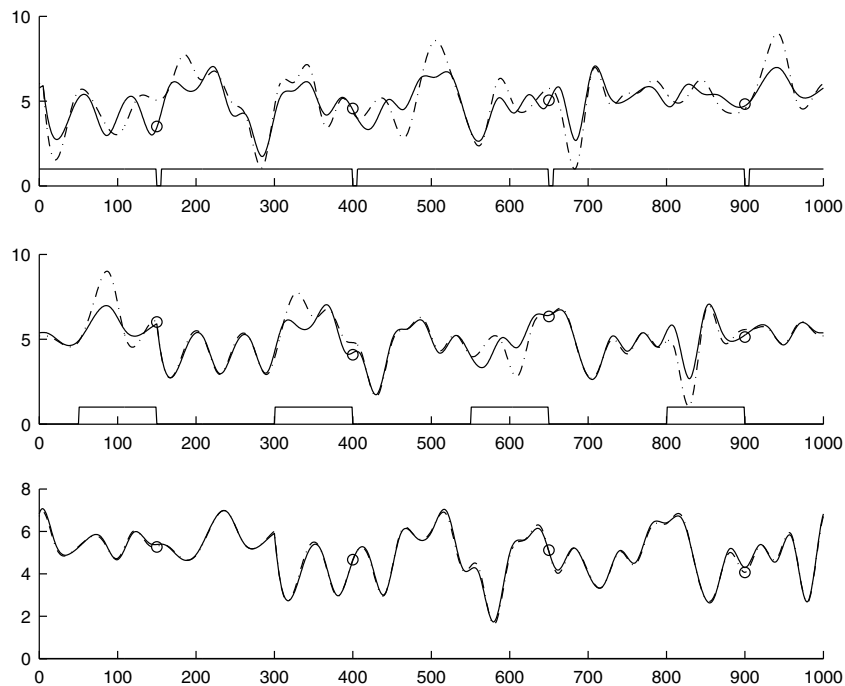
Fig. 1. Results of the EnKF to the model problem (50) at three different times $t = 5$ (top figure), $t = 150$ (middle figure), and $t = 300$ (bottom figure). Solid lines are the true solution Ψ^t, circles are the measurements d, dashed lines are the mean of the EnKF estimates $\widehat{\Psi}^a$, and another set of solid lines near the bottom of each figure are the standard deviations of the EnKF.
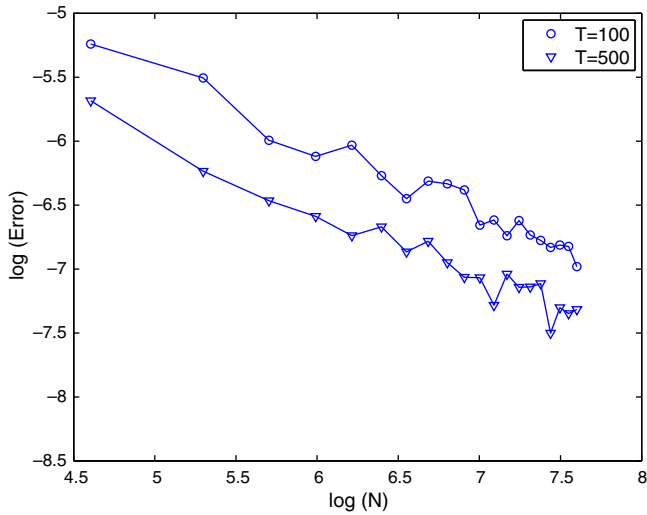
Fig. 2. Error convergence of the EnKF with increased sample size N.
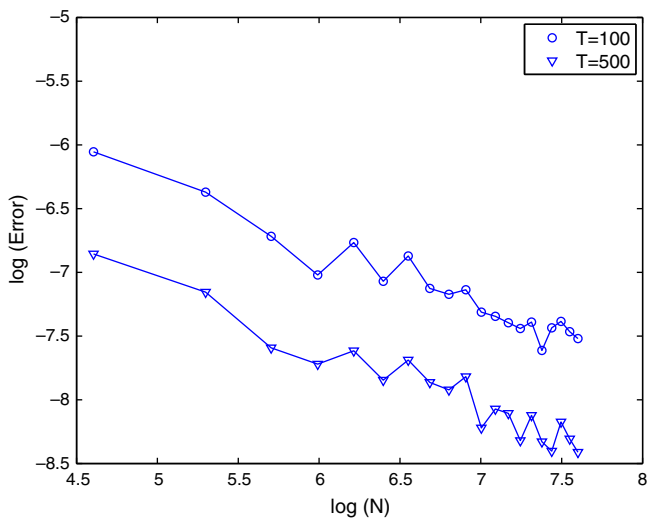
Fig. 3. Error convergence of the EnSRF with increased sample size N.

mean of the EnKF estimates converge to the true state as time evolves, and the standard deviation of the EnKF estimates converge to the standard deviation of the measurements, which is 0.1 and can not be seen visually in the bottom figure.

Next we examine the global error convergence (38) with respect to the ensemble size N. Fig. 2 illustrates the error at two different time of $t = 100$ and $t = 500$. It can be seen that the errors decay as the ensemble size N increases, and the rate of convergence is approximately $N^{-1/2}$. This is consistent with the error analysis from (38). The convergence of the EnSRF at $t = 100$ and $t = 500$ are shown in Fig. 3, and we observe a similar rate of convergence. Note that the errors of EnSRF are smaller than those of EnKF. This is because of the elimination of the error in sampling the measurements.

We further examine the numerical error dependence on the error ϵ^{f} defined in (29). In this problem there is no modelling error, therefore $\|\epsilon^{f}\| = \|\epsilon\|$ and can be measured by the standard deviation of the measurement errors. Following the error bound (38 and (30), the numerical error should be proportional to the standard deviation of the measurement errors.

The numerical errors with different levels of standard deviation of the measurement errors are shown in Figs. 4 and 5, for the EnKF and EnSRF, respectively. The almost linear dependence of numerical errors on the standard deviations of the measurement errors can be seen clearly, consistent with the result from analysis. The time evolution of numerical errors of the EnSRF is much smoother and smaller, compared to that of the EnKF.

5.3. Results of the qEnKF

Here we examine the performance of the qEnKF, the ensemble Kalman filter based on deterministic sampling of cubature. In particular, we employ the degree two formula (48) and degree three formula (49) as the deterministic sampling ensemble, and denote the corresponding method qEnKF-2 and qEnKF-3, respectively. For the model problem studied here, the qEnKF-2 requires $N = n + 1 = 51$ sampling points and the qEnKF-3 requires $N = 2n = 100$ points. In Fig. 6, the error evolution in time of the qEnKF methods are plotted, along with that of the EnKF with different ensemble size. It is observed that with the same ensemble size, the qEnKF-3 is more accurate than the traditional EnKF with $N = 100$. The improvement is, however, marginal, and the qEnKF-2 with less number of points ($N = 51$) has larger errors. The reason
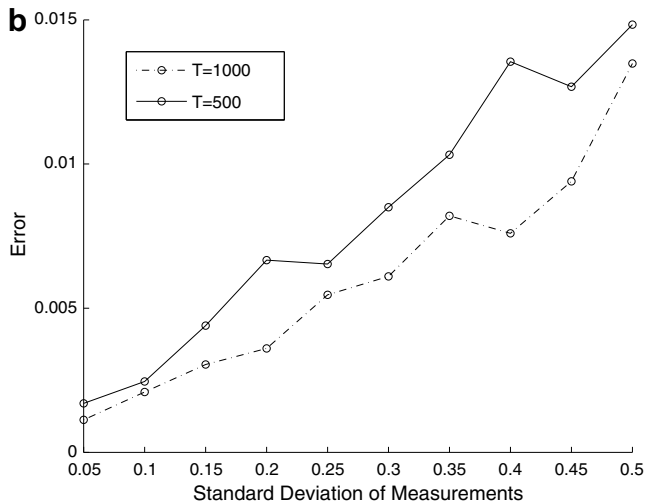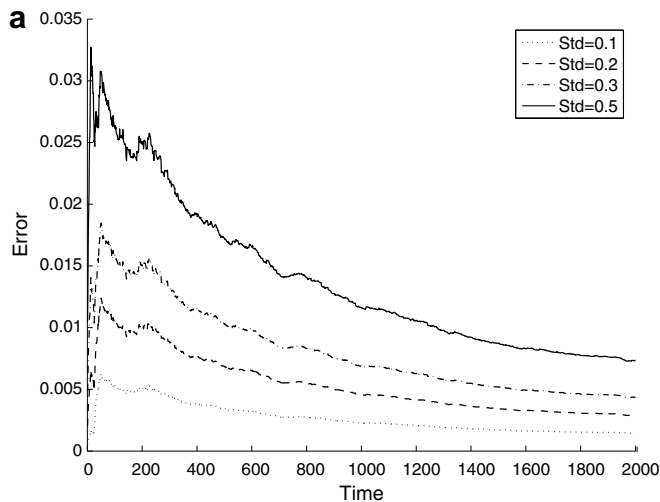
Fig. 4. Numerical errors of the EnKF with measurement errors of different standard deviations. (a) Time evolution of the numerical errors; (b) numerical errors at $t = 500$ and $t = 1000$.

a

b
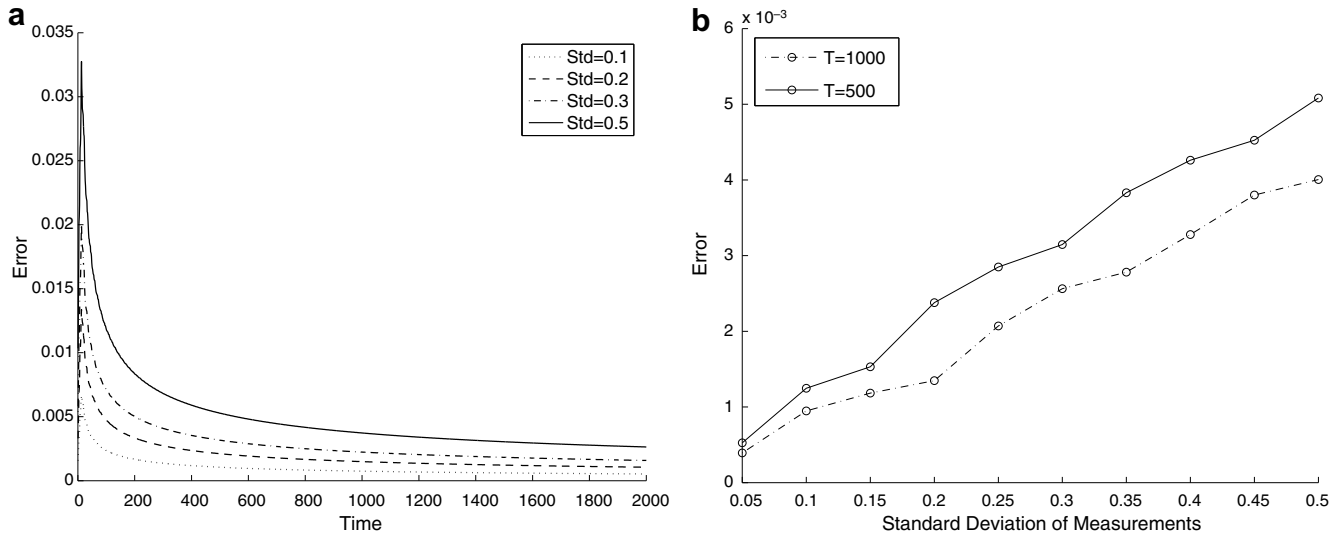
Fig. 5. Numerical errors of the EnSRF with measurement errors of different standard deviations. (a) Time evolution of the numerical errors; (b) numerical errors at $t = 500$ and $t = 1000$.
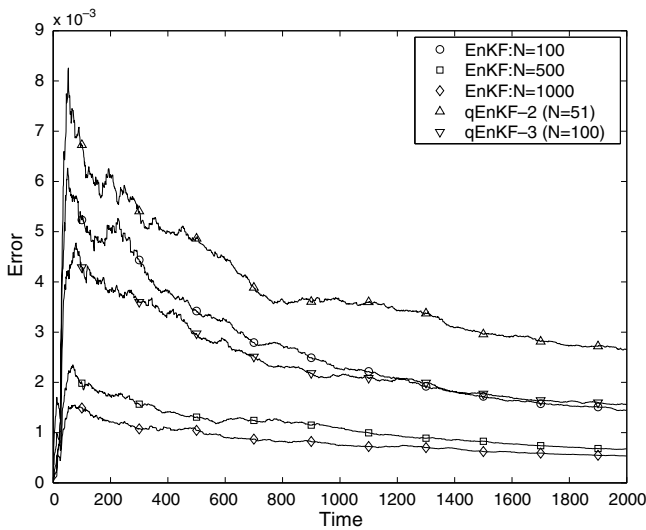
Fig. 6. Global error evolution over time of the EnKF with different ensemble size of $N = 100$, $N = 500$ and $N = 1000$, the qEnKF-2 ($N = 51$) and the qEnKF-3 ($N = 100$).
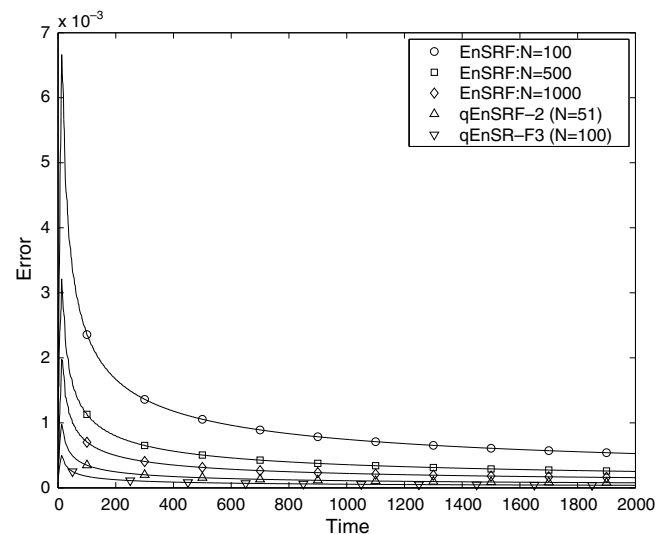
Fig. 7. Global error evolution over time of the EnSRF with different ensemble size of $N = 100$, $N = 500$ and $N = 1000$, the qEnSRF-2 ($N = 51$), and the qEnSRF-3 ($N = 100$).

the advantage of qEnKF is not obvious is due to the existence of the ensemble errors in sampling the measurements, which is present and becomes dominant. Next we employ the EnSRF approach (45) to eliminate the errors in sampling the measurements and combine it with the cubature sampling strategy. The corresponding approaches, termed qEnSRF-2 and qEnSRF-3, require the same number of sampling points as those of qEnKF-2 and qEnKF-3. The error evolution in time is shown in Fig. 7. It is observed that the errors are much smaller and smoother, indicating much improved accuracy.

The errors are tabulated in Table 1, for the EnKF, EnSRF and qEnSRF. It is seen that the qEnSRF methods offer much better accuracy. The qEnSRF-3, with only $N = 100$ sampling points, is more accurate than the EnSRF with ensemble size as large as $N = 10^4$. Even qEnSRF-2, which requires $N = 51$ samples, is comparable to EnSRF with $N = 10^4$. Note in all these approaches the computational costs are directly determined by the size of ensemble. Therefore the qEnSRF methods offer an efficient alternative for more accurate

data assimilation, especially when the computational cost of (1) is of great concern.

5.4. Error dependence on assimilation frequency

Here we examine the impact of the size of assimilation step (ΔT) on numerical accuracy. As suggested by the error analysis (38),

Table 1
Comparison of numerical errors of the EnKF, EnSRF and qEnSRF

	$t = 100$	$t = 500$	$t = 1000$	$t = 1500$
EnKF $N = 100$	5.3×10^{-3}	3.4×10^{-3}	2.3×10^{-3}	1.7×10^{-3}
EnKF $N = 10^3$	1.5×10^{-3}	1.0×10^{-3}	7.4×10^{-4}	6.2×10^{-4}
EnKF $N = 10^4$	4.6×10^{-4}	2.8×10^{-4}	2.4×10^{-4}	1.9×10^{-4}
EnSRF $N = 100$	2.3×10^{-3}	1.1×10^{-3}	7.0×10^{-4}	6.0×10^{-4}
EnSRF $N = 10^3$	7.0×10^{-4}	3.0×10^{-4}	2.0×10^{-4}	2.0×10^{-4}
EnSRF $N = 10^4$	2.2×10^{-4}	9.6×10^{-5}	6.8×10^{-5}	5.6×10^{-5}
qEnSRF-2 ($N = 51$)	3.5×10^{-4}	1.6×10^{-4}	1.1×10^{-4}	9.0×10^{-5}
qEnSRF-3 ($N = 100$)	1.8×10^{-4}	7.9×10^{-5}	5.6×10^{-5}	4.6×10^{-5}

Fig. 8. Accuracy of various EnKF schemes with different size of assimilation step ΔT. (a) EnKF and EnSRF with $N = 100$; (b) qEnSRF methods.
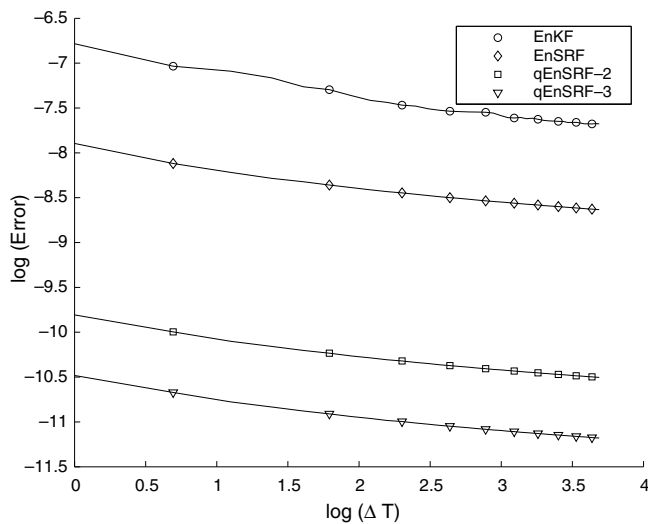
Fig. 9. Comparison of the accuracy of various EnKF schemes with different size of assimilation step ΔT.

more frequent assimilation with smaller ΔT may lead to larger numerical errors in the EnKF approaches. This is evident in Fig. 8, where the numerical errors of the different sampling approaches are shown with different assimilation step ΔT ranging from 1 to 40. The errors are reported at large time $t = 4000$ so that all simulations have been sufficiently assimilated. We observe clearly the larger errors at smaller ΔT. Such inverse dependence of numerical errors on ΔT is independent of the choice sampling strategy, as shown in Fig. 9 where results of EnKF, EnSRF, and qEnSRF are plotted in comparison. From the log–log scale it can be concluded that different approaches have a same rate of the inverse error dependence on the size of ΔT. Again, the much improved accuracy of qEnSRF is obvious with the same computational cost ($N = 100$).

6. Conclusion

In this paper we conduct rigorous analysis on the numerical errors of the ensemble Kalman filter (EnKF). The results indicate that the numerical errors consist of the classical discretizational errors for solving the underlying model equations and the ensemble errors for sampling the model states and measurements. The sam-

pling errors of measurements can be eliminated by using the ensemble square root filter (EnSRF), and the errors of sampling model states can be significantly reduced by using deterministic sampling methods based on cubature rules (qEnKF). Examples are presented for a model problem, where we focus the numerical errors associated with sampling. The results verify the theoretical analysis and demonstrate that the qEnSRF, a combination of the EnSRF and qEnKF, can significantly reduce the sampling errors in model state estimates and therefore provides an efficient methodology for data assimilation. The error estimate also indicates that more frequent data assimilation can lead to larger numerical errors in the EnKF approaches, regardless the specific sampling strategy. This result, verified by the numerical tests, suggests that in practice the choice of assimilation step should be a balance between better estimates of the true states by using more frequent assimilation (whenever measurement data is available) and smaller numerical errors by using less frequent assimilation. Future research will include more extensive studies and performance evaluations of the qEnKF for more complex and nonlinear problems.

References

[1] C.H. Bishop, B.J. Etherto, S.J. Majumdar, Adaptive sampling with the ensemble transform Kalman filter, part i: theoretical aspects, Mon. Weather Rev. 129 (2001) 420–436.
[2] G. Burgers, P.V. Leeuwen, G. Evensen, Analysis scheme in the ensemble Kalman filter, Mon. Weather Rev. 126 (1998) 1719–1724.
[3] S.E. Cohn, An introduction to estimation theory, J. Meteor. Soc. Jpn. 75 (1997) 257–288.
[4] R. Cools, An encyclopaedia of cubature formulas, J. Complex. 19 (2003) 445–453.
[5] P.J. Davis, Interpolation and Approximation, Dover, 1975.
[6] H. Engels, Numerical Quadrature and Cubature, Academic Press, 1980.
[7] G. Evensen, Sequential data assimilation with a nonlinear quasi-geostrophic model using Monte Carlo methods to forecast error statistics, J. Geophys. Res. 99 (1994) 10143–10162.
[8] G. Evensen, The ensemble Kalman filter: theoretical formulation and practical implementation, Ocean Dyn. 53 (2003) 343–367.
[9] G. Evensen, Sampling strategies and square root analysis schemes for the EnKF, Ocean Dyn. 54 (2004) 539–560.
[10] G. Evensen, Data Assimilation, the Ensemble Kalman Filter, Springer-Verlag, Berlin, 2007.
[11] A. Gelb, Applied Optimal Estimation, MIT Press, Cambridge, 1974.
[12] S. Haber, Numerical evaluation of multiple integrals, SIAM Rev. 12 (4) (1970) 481–526.
[13] A.H. Jazwinski, Stochastic Processes and Filtering Theory, Academic Press, San Diego, CA, 1970.
[14] R. Kalman, R. Bucy, New results in linear prediction and filter theory, Trans. AMSE J. Basic Engrg. 83D (1961) 85–108.

[15] L. Nerger, Parallel filter algorithms for data assimilation in oceanography, Reports on Polar and Marine Research 487. Ph.D. Thesis, Alfred Wegener Institute for Polar and Marine Research, University of Bremen, Bremerhaven, Germany, 2004.

[16] D.T. Pham, Stochastic methods for sequential data assimilation in strongly nonlinear systems, Mon. Weather Rev. 129 (2001) 1194–1207.

[17] A. Quarteroni, R. Sacco, F. Saleri, Numerical Mathematics, Springer-Verlag, New York, 2000.

[18] A.H. Stroud, Approximate Calculation of Multiple Integrals, Prentice-Hall, Englewood Cliffs, NJ, 1971.

[19] M.K. Tippett, J.L. Anderson, C.H. Bishop, T.M. Hamill, J.S. Whitaker, Ensemble square-root filters, Mon. Weather Rev. 131 (2003) 1485–1490.

[20] J.S. Whitaker, T.M. Hamill, Ensemble data assimilation without perturbed observations, Mon. Weather Rev. 130 (2002) 1913–1924.

[21] D. Xiu, Numerical integration formulas of degree two, Appl. Numer. Math. (2007), doi:10.1016/j.apnum.2007.09.004.